LAND DEGRADATION & DEVELOPMENT
Land Degrad. Develop. (2013)
Published online in Wiley Online Library (wileyonlinelibrary.com) **DOI**: 10.1002/ldr.2253

MODELING INTERRILL EROSION ON UNPAVED ROADS IN THE LOESS PLATEAU OF CHINA

Longxi Cao[1,2], Keli Zhang[2]*, Hailun Dai[2], Yin Liang[1]

[1]*Key Laboratory of Soil Environment and Pollution Remediation, Institute of Soil Science, Chinese Academy of Sciences, Nanjing, PR China*
[2]*State Key Laboratory of Earth Surface Processes and Resource Ecology, School of Geography, Beijing Normal University, Beijing, PR China*

Received: 10 March 2013; Revised: 5 September 2013; Accepted: 6 September 2013

ABSTRACT

Unpaved roads play an important role in soil loss in small watersheds. In order to assess the impact of these unpaved roads in the Loess Plateau of China, runoff and sediment yields from road-related sources must be quantified. Field rainfall simulation experiments were conducted under three slope gradients and five rainfall intensities on unpaved loess roads in a small watershed. Results showed that the runoff generation was very fast in loess road surface (time to runoff < 1 min) and produced a high runoff coefficient (mean value $> 0{\cdot}8$). Soil loss rates were decreased as surface loose materials were washed away during a rainstorm. Rainfall intensity, initial soil moisture, and slope gradient are key factors to model surface runoff and sediment yield. Soil loss on loess road surface could be estimated by a linear function of stream power ($R^2 = 0{\cdot}907$). Four commonly interrill erosion models were evaluated and compared, and the interrill erodibility adopted in the Water Erosion Prediction Project model was determined as $1{\cdot}34 \times 10^6$ (kg s m^{-4}). A new equation taking into account different parameters like rainfall intensity, surface flow discharge, and slope gradient was established. Copyright © 2013 John Wiley & Sons, Ltd.

KEYWORDS: unpaved road; interrill erosion; runoff; rainfall simulation; the Loess Plateau; China

INTRODUCTION

During the last century, rural roads have been greatly expanded (Leh *et al*., 2013). It is well known that unpaved rural roads contribute significantly to soil loss in agricultural watersheds despite representing a small fraction of watershed-occupied areas (Dunne, 1979). Comparing with other agricultural land, sealed road surfaces may increase the generation of Hortonian overland flow by decreasing soil infiltration capacity and increasing the production of loose materials as caused by heavy traffic (Dunne, 1979; Ziegler *et al*., 2000b; Croke & Mockler, 2001). Recently, exacerbated soil losses after roads constructions have been reported in many parts of the world, including USA, England, Kuwait, Norway, South Africa, Tunisia, and China (Leh *et al*., 2013; Posthumus *et al*., 2011; Al-Awadhi, 2011; Tømmervik *et al*., 2012; Foster *et al*., 2012; Desprats *et al*., 2013; Xu *et al*., 2009). Particularly in the Loess Plateau of China, where general sediment yields have been partly controlled by conservation practices (Zhao et *al*., 2013), unpaved road networks play an increasingly important role in sediment generation at catchment scale (Cao *et al*., 2009; Liu *et al*., 2010). A quantitative description of runoff and sediment yields from road-related sources is therefore critical (Xu *et al*., 2009).

Road-related erosion can be monitored at different scales and evaluated by different approaches (Desprats *et al*., 2013). Field monitoring under natural rainfall conditions is the conventional method to study runoff characteristics and sediment yield from road sediment sources (Reid & Dunne, 1984; Luce & Black, 1999; MacDonald *et al*., 2001; Xu *et al*., 2009). However, accurate measurements of the soil loss process during natural rainstorms are nearly impossible. Rainfall simulation is thus an efficient complementary method, which has the advantage of being less time consuming, more controlled, and lower in cost (Meyer, 1994). In spite of the limitations such as small plot scale, simulated rainfall has been adopted to explore road-related runoff and soil loss processes throughout the world (Elliot *et al*., 1995; Croke *et al*., 1999; Ziegler *et al*., 2000b; Arnáez *et al*., 2004). These studies have described the characteristics of road-related runoff and the sediment generation process (Croke *et al*., 1999; Ziegler *et al*., 2000b; Arnáez *et al*., 2004; Cerdà, 2007), compared soil loss rates for different portions of unpaved roads (Jordán & Martínez-Zavala, 2008; Jordán *et al*., 2009), and analyzed the seasonal variability of road-related runoff and soil loss (Martínez-Zavala *et al*., 2008). Many studies have also shown that soil erosion models can provide reasonable estimations of runoff and erosion from road surfaces (Elliot *et al*., 1995). A growing body of research has focused on rainfall simulation model application and validation for unpaved roads (Elliot *et al*., 1995; Ziegler *et al*., 2001), and factors such as road surface interrill erodibility have been explored (Ziegler *et al*., 2000a; Sheridan *et al*., 2008; Foltz *et al*., 2009).

These studies have made progress on the quantification of the road surface soil loss process. However, most of the

* Correspondence to: K. Zhang, State Key Laboratory of Earth Surface Processes and Resource Ecology, School of Geography, Beijing Normal University, No. 19, Xinjiekou Wai Street, Beijing 100875, PR China.
E-mail: keli@bnu.edu.cn

experiments were conducted on relatively low slope gradients (less than 26·8%), whereas the landform in the Loess Plateau is characterized by its steep slope gradient (Cao *et al*., 2011). Soil loss predicting equations can lead to large errors when extrapolated beyond the range of slope gradients, which used to generate the equations (Liu *et al*., 1994). Thus, the existing relationships cannot be used without modification in the evaluation of road erosion for the Loess Plateau. Liu *et al*. (2010) constructed 26·8% slope loess road sections in the laboratory and studied the efficacy of grass on mitigating runoff and erosion under simulated rainfall. However, the laboratory conditions are different from real unpaved roads in vehicle disturbance and compaction. Furthermore, their experiments were conducted using just one slope gradient; therefore, they are unable to represent the worth of different slope gradients on runoff generation and road surface soil loss. Cao *et al*. (2011) have conducted field runoff simulation experiments on unpaved loess road surfaces and calculated rill erodibility, enabling a prediction of soil loss. However, the prediction of interrill erosion of loess road surfaces has not been well addressed. Hence, experiments carried out on unpaved road surfaces with different slope gradients are still needed. Parametric models need to be developed in order to use erosion models such as Water Erosion Prediction Project (WEPP) on road surfaces.

The objectives of this study were to: (i) study the characteristics of runoff and sediment generation processes; and (ii) develop equations and quantify parameters that can be helpful in predicting interrill soil loss on loess road surfaces. The results provide a background for developing a physically based model for erosion of unpaved roads on the Loess Plateau of China.

MATERIAL AND METHODS

Study Area

All experiments were performed on surfaces of unpaved loess roads in the Danangou watershed near the Ansai Research Station of Soil and Water Conservation, Chinese Academy of Sciences, which is located in the center of the Loess Plateau of China (36°53′N, 109°19′E). The average temperature is 8·8 °C, and monthly averages range from 22·5 °C in July to −7 °C in January. The annual precipitation is 562 mm, and 60% of the rainfall occurs between July and September. The watershed has an altitude between 1,000 and 1,350 m asl; the topography is sharply ridged, and hills rise and fall abruptly. The soil has been developed from loess (Zhao *et al*., 2013), which is prone to erosion; its erosion rate is high and estimated as 100–120 Mg ha^{-1} yr^{-1} from the catchment measurement (Song *et al*., 1989). The study area is an agricultural watershed in which large numbers of unpaved roads are constructed for farming, quarrying, and other activities. Determined by the underlying topography, steep road sections can be found throughout the watershed. During a rainstorm, runoff and sediment are commonly rerouted and enhanced by road networks (Xu *et al*., 2007).

Experiments were conducted on a 3-m-wide unpaved orchard road from August to September 2009. The road was constructed for harvesting purposes 10 years before the experiments were carried out by moving surface soil downhill using a crawler tractor; in the process, road surface was compacted. The road only received occasional disturbance by small vehicles during the harvest. Thus, it could be classified as a secondary road according to Cao *et al*. (2009). Three segments with slope gradients of 10·5%, 17·6%, and 26·8% were selected to represent roads on gentle, mild, and steep slopes in the study area, respectively. There was no evidence of wheel tracks or rills on road surfaces. Soil texture near the experiment site was 10·25% sand (2–0·05 mm), 72·10% silt (0·05–0·002 mm) and 17·65% clay (Fu *et al*., 2003).

Rainfall Simulation Experiments

Experiments were carried out using a rainfall simulator that was modified on the basis of Meyer & Harmon (1979). As shown in Figure 1, the 2·5-m-long trough rainfall simulator was set with steel frame in the direction of the road. Three Spraying Systems Veejet 80100 nozzles (Spraying Systems Co. Wheaton, Illinois, USA) were assembled with 1·1 m interval on the trough with a water pressure of 40 kPa. Nozzles could swing and generate continuous rainfall intensity. The swing frequency could be changed by an impulse signal through a controller. In this way, rainfall intensity could be changed automatically. Water not sprayed to the plot was recirculated within the trough. When the nozzles reached a height of 2·5 m, simulated rainfall intensity showed a high spatial uniformity (Xie *et al*., 2008). According to our calibration results, the uniformity coefficient (1 standard deviation/mean) of rainfall intensity was calculated as 0·9 within the 1·1 m^2 rectangular area (50 × 220 cm) that was directly under the rainfall simulator. The rectangular area was marked on the road surface, and the plot boundaries were defined by connecting 30-cm-length and 15-cm-height iron sheets together. Because the compacted road surface was firm and

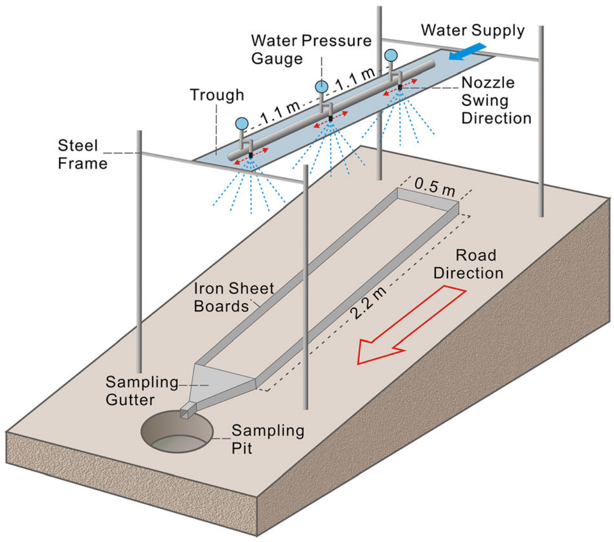

Figure 1. Sketch and construction of the experimental field plot. This figure is available in colour online at wileyonlinelibrary.com/journal/ldr.

was also easily disturbed, iron sheets were folded into an "L" shape and fixed to the road surface by mud. A 15-cm-height wooden plank was then placed at the higher end to prevent water from flowing into the plot. A gutter was placed at the lower end of the plot to collect runoff and sediment samples. Finally, clear water was supplied through a 2·5-cm-diameter fire nylon hose by a 370 W pump. The pump and the rainfall simulator were driven by a 3·6 kW 220 V gasoline generator. Rainfall intensity in this study was set at 43·8, 68·4, 83·4, 128·4, and 142·2 mm h^{-1}.

Experimental Design

Before each experiment, three soil samples were taken using an iron cylinder (5 cm height and 5 cm diameter) along the plot edge. Soil samples were then oven-dried at 105 °C for 24 h to measure soil moisture and bulk density. The slope angle of each plot was determined using a clinometer. For each experiment, a rainfall simulation thunderstorm was performed for 30 min, and surface runoff was collected and measured by sampling bottles at 1-min intervals. The sampling duration was recorded to determine the flow rate. Sampled sediment was oven-dried at 105 °C for 24 h to determine the runoff sediment concentration. By integrating the runoff and sediment concentration over time, total runoff and soil loss were determined. Each plot was used once, and new plots were set on different undisturbed surfaces to achieve the same initial conditions. Finally, 15 valid experiments comprising the combination of five rainfall intensities and three slope gradients were conducted.

Consolidated and compacted road surfaces have been reported hard to be detached and need relatively high critical shear stress to initiate rills (Cao *et al.*, 2009). Because of the small scale and the short length of the field plots, no rill erosion was expected on the experimental road surfaces. The processes during rainfall simulation could thus be treated as interrill erosion, which was mainly caused by raindrop splash and overland flow transportation. The small size of the plots allows measurements of soil erodibility, infiltration, and runoff, which are representative of the interrill scale soil erosion processes (Cerdà, 1998; Cerdà *et al.*, 2009). Considering the difficulty of accurately measuring surface hydraulic parameters such as runoff speed in interrill areas, the stream power concept was applied, obviating the need for runoff speed data (Nearing *et al.*, 1997). It was calculated as follows (Hairsine & Rose, 1992):

$$\omega = \rho g S q \tag{1}$$

where ω is stream power (g s^{-3}), ρ is density of water (g cm^{-3}), g is gravitational constant (cm s^{-2}), S is slope gradient (m m^{-1}), and q is unit discharge of runoff (cm^2 s^{-1}). Stream power is the factor that affects the effect of both slope steepness and runoff rate on soil loss (Huang, 1995).

Four generally used interrill erosion models were applied in order to explore interrill erodibility and predict soil loss on the loess road surface. The equation and source of each model is described in Table I. Among them, model 1 was adopted in the WEPP model to predict interrill erosion.

Data Analysis

The effects of slope steepness, soil water content, and bulk density on road surface runoff and soil loss were analyzed. The Pearson correlation coefficient was used to evaluate the relationship between hydrological and soil loss parameters and the influencing factors. Results were reported at the $\alpha = 0{\cdot}05$ level of significance. The coefficient of determination (R^2) and model efficiency (ME) was used to evaluate the performance of the applied models. ME was calculated using the following equation (Nash & Sutcliffe, 1970):

$$ME = 1 - \frac{\sum (Q_i - Q_c)^2}{\sum (Q_i - Q_m)^2} \tag{2}$$

where ME is model efficiency, an ME value of 1 indicates perfect agreement between measured and calculated values and an ME value of <1 indicates a less strong correlation, Q_i is the measured value, Q_c is the calculated value, and Q_m is the mean value of the measured values. All the analyses and graphical displays were made using the IBM SPSS STATISTICS 19·0 (IBM Corp., 2010) and ORIGIN (OriginLab, Northampton, MA, USA) software packages respectively.

RESULTS AND DISCUSSION

Runoff Response

During the 30-min rainfall simulation, runoff coefficient for all of the experiments increased rapidly within the first 3–5 min and leveled out as the result of surface saturation and sealing (Figure 2 shows a typical runoff sequence). Indices to describe runoff response for each experiment were calculated and pooled in Table II. It can be seen that time to runoff on all plots was less than 1 min, with the shortest on the 26·8% slope (ranging from 15 to 33 s with the mean value of 23 s). Both flow rate and runoff coefficient showed slightly

Table I. Models applied to predict interrill soil loss

Model	1	2	3	4
Equation	$D_i = K_i I Q S_f$	$D_i = K_i I Q S$	$D_i = K_i I Q S^{2/3}$	$D_i = K_i I Q^{1/2} S^{2/3}$
Source	Flanagan & Nearing (1995)	Kinnell (1993)	Bulygin *et al.* (2002)	Zhang *et al.* (1998)

Where D_i is the delivery of sediment from interrill areas (kg s^{-1} m^{-2}), K_i is interrill erodibility (kg s m^{-4}), I is the effective rainfall intensity (m s^{-1}), Q is the runoff rate averaged over the entire runoff interval (m s^{-1}), S is slope gradient (m m^{-1}), and S_f is a slope adjustment factor given by: $S_f = 1{\cdot}05 - 0{\cdot}85e^{-4\sin\theta}$, where θ is the slope gradient of the surface toward a nearby rill, which equals to the slope gradient of the plot in this study.

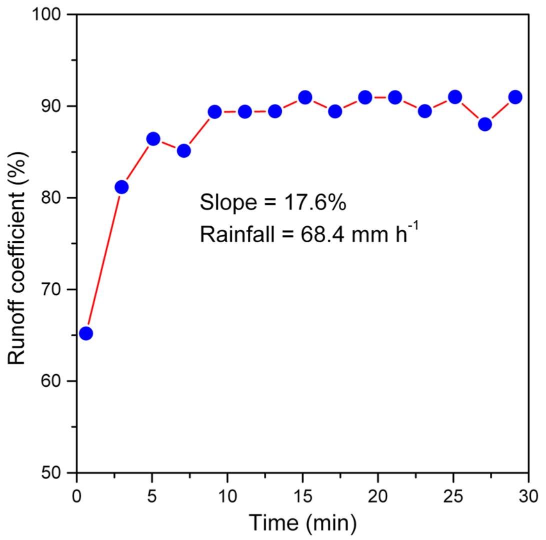

Figure 2. Road surface runoff coefficient from a typical rainfall simulation. This figure is available in colour online at wileyonlinelibrary.com/journal/ldr.

ascending trend with slope gradient. In general, runoff coefficient was high on all plots with the mean value higher than 0·8.

In order to better explore the factors influencing road surface runoff response, a Pearson correlation was carried out (Table III); this showed that runoff rate, time to runoff, and runoff coefficient were significantly correlated to rainfall intensity and initial soil moisture. However, surface runoff response was statistically independent of slope gradient and bulk density.

Soil Loss Response

Soil loss is shown in Figure 3. Almost all curves showed the highest soil loss rates at the first sample. Soil loss rate decreased with time as the loose materials were washed away. With the same slope gradient, soil loss would usually be intensified as the rainfall intensity increased. This implies that high-intensity rainstorms have a strong ability to splash and transport soil particles; additionally, sealed road surface would accelerate runoff flow and therefore enhance soil loss. On the other hand, soil loss curve under high rainfall intensities would decrease more quickly than that under the low rainfall intensities. As the slope gradients increased, the gaps between soil loss rates of different rainfall intensities would be enlarged. On the 26·8% slope, soil loss rate under the 142·2 mm h^{-1} rainfall was one order of magnitude higher than that under the 43·8 mm h^{-1} rainfall. Table II showed that the average soil loss rates were increased with slope gradients. Plots on the 26·8% slope had the highest soil loss rate (mean value 0·436 g s^{-1} m^{-2}, ranging from 0·097 to 0·877 g s^{-1} m^{-2}) among all plots tested.

A Pearson correlation showed that soil loss rate was most significantly related to both runoff rate and rainfall intensity (Table IV). Soil moisture and runoff coefficient were also found to be significantly correlated with soil loss rate. The high soil moisture and runoff coefficient indicated that more overland flow had been generated and more soil detached particles were transported to the outlet of the plot. Nevertheless, both slope gradient and soil bulk density were only weakly correlated with soil loss rate.

Figure 4 shows the relationship between soil loss rate and runoff rate. It has been demonstrated that soil loss rate was linearly increased with runoff rate for the 10·5% slope. When the slope gradient increased, the relationship between soil loss rate and runoff rate changed into power trend, and the exponent value also increased. The rising function exponent showed the increasing erosion intensity on steep slopes. It reflected the aforementioned road surface erosion intensification on steep slopes.

Soil Loss Prediction and Model Development

Stream power has been included in models for sediment entrainment and transport under conditions of shallow flow and rill erosion. The following equation was used to estimate soil loss in our study:

$$q_s = 0{\cdot}00008\omega - 0{\cdot}00079 \quad \mathrm{N} = 15 \quad \mathrm{R}^2 = 0{\cdot}907 \qquad (3)$$

where q_s is the unit sediment load (g s^{-1} cm^{-1}), and ω is stream power (g s^{-3}).

Table II. Road surface characteristics and indices of runoff and soil loss with different slope gradients[a]

Variables		10·5% Slope	17·6% Slope	26·8% Slope
Initial soil moisture (g g^{-1})	Mean	0·155	0·160	0·174
	Standard deviation	0·012	0·023	0·024
Bulk density (g m^{-3})	Mean	1·594	1·569	1·515
	Standard deviation	0·047	0·031	0·032
Time to runoff (s)	Mean	24·2	29·4	23·0
	Standard deviation	11·30	11·93	6·89
Runoff rate (L s^{-1})	Mean	0·0242	0·0250	0·0255
	Standard deviation	0·012	0·012	0·012
Runoff coefficient (%)	Mean	84·5	86·5	88·5
	Standard deviation	6·28	4·22	4·46
Soil loss rate (g s^{-1} m^{-2})	Mean	0·228	0·281	0·436
	Standard deviation	0·126	0·162	0·321

[a]Total runoff volume and soil loss for each experiment were obtained by integrating sampled runoff and sediment concentration over time. In turn, runoff rate was calculated as total runoff volume divided by experiment time, runoff coefficient was calculated as total runoff volume divided by total rainfall volume, and soil loss rate was calculated as total soil loss divided by experiment time and plot area.

Table III. Pearson correlation between time to runoff, runoff coefficient, and the effective factors

		Rainfall intensity	Initial soil moisture	Slope	Bulk density
Runoff rate	Pearson *r*	0·995	0·532	0·067	−0·245
	P (two-tailed)	<0·001*	0·041*	0·813	0·38
	N	15	15	15	15
Time to runoff	Pearson *r*	−0·875	−0·545	−0·087	0·246
	P (two-tailed)	<0·001*	0·036*	0·758	0·377
	N	15	15	15	15
Runoff coefficient	Pearson *r*	0·543	0·61	0·268	−0·201
	P (two-tailed)	0·036*	0·016*	0·334	0·472
	N	15	15	15	15

*Marked *p*-values are significant (< 0·05).

Corresponding to the interrill erosion model adopted in WEPP (model 1 in Table I), linear regression analysis with zero intercept was developed between soil loss rate and rainfall characteristics and topography (IQS_f):

$$D_i = 1335793\, IQS_f \quad R^2 = 0{\cdot}814 \tag{4}$$

where D_i is the delivery of sediment from interrill areas ($\mathrm{kg\,s^{-1}\,m^{-2}}$), I is the effective rainfall intensity ($\mathrm{m\,s^{-1}}$), Q is the average runoff rate over the entire runoff interval ($\mathrm{m\,s^{-1}}$), and S_f is a slope adjustment factor. The interrill erodibility on the loess road surface was $1{\cdot}34 \times 10^6$ ($\mathrm{kg\,s\,m^{-4}}$) based on the coefficient of regression equation.

Linear regressions with zero intercept were also carried out for other three selected models (models 2, 3, and 4 in Table I). Regression equations and ME were listed in Table V. Models 1, 2, and 3 in Table V are essentially the same except for different slope factors. The better performance of model 2 over the other two models indicated that the linear slope factor was better than either convex curvilinear or power slope factors in describing the effect of slope steepness for this data set. Similarly, the fact that model 4 was better than model 3 implied that the square root runoff factor was superior to the linear runoff factor. On the basis of the outstanding factors in the selected models, a new equation for road surface interrill erosion prediction was therefore developed (Equation 5).

$$D_i = 12536{\cdot}15\, IQ^{1/2}S \quad ME = 0{\cdot}945 \tag{5}$$

where D_i is the delivery of sediment from interrill areas ($\mathrm{kg\,s^{-1}\,m^{-2}}$), I is the effective rainfall intensity ($\mathrm{m\,s^{-1}}$), Q is unit discharge ($\mathrm{m\,s^{-1}}$), and S is slope gradient ($\mathrm{m\,m^{-1}}$). The one-to-one line plotted in Figure 5 shows impressive agreement between estimations and observations. The ME value of Equation 5 is higher than all selected models in Table V. It means that the new equation could provide estimations that are very close to measured soil loss rates. Therefore, in this study, Equation 5 is superior to selected models in predicting interrill erosion of unpaved loess road surface.

Implications of the High Erosion Rates on Roads

Unpaved roads can highly modify the hydrological behavior of hillslopes (Jordán *et al*., 2009). In this study, the short time to runoff and high runoff coefficient showed an acceleration of runoff generation due to road surface compaction. The longer time to runoff on 17·6% slope might be attributed to the plot surface morphology that delayed the flow generation. That is, surface roughness would provide water surface storage in the depressions and alter the flow direction on the surface (Darboux *et al*., 2001). The slightly ascending trend of flow rate and runoff coefficient reflects the fact that surface runoff would increase with the increase of slope steepness (Morgan, 2005). Generally, when conditions are homogeneous, slope gradient and bulk density would be expected to be positively correlated with the runoff coefficient (Commandeur, 1992). However, runoff response was statistically independent of slope gradient and bulk density on road surface of this study. This unusual finding

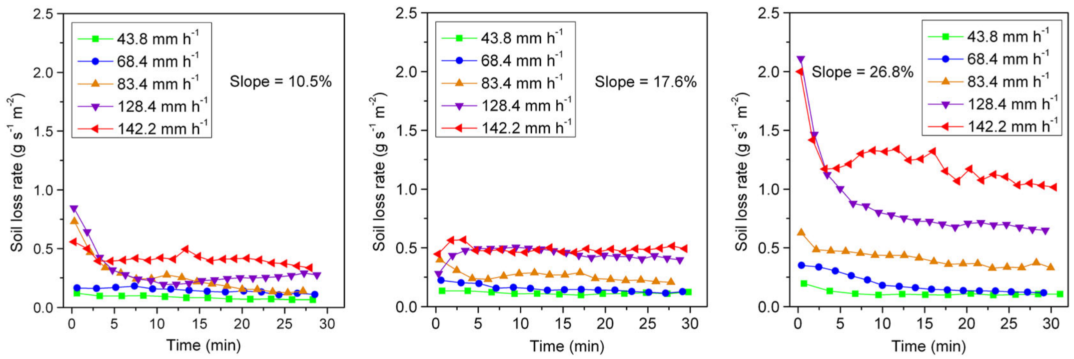

Figure 3. Road surface soil loss rates from rainfall simulations on different plots. This figure is available in colour online at wileyonlinelibrary.com/journal/ldr.

Table IV. Pearson correlation between soil loss rate and the effective factors

		Slope	Rainfall intensity	Runoff rate	Initial soil moisture	Bulk density	Runoff coefficient
Soil loss rate	Pearson *r*	0·421	0·824	0·842	0·711	−0·456	0·565
	P (two-tailed)	0·118	<0·001*	<0·001*	0·003*	0·087	0·028*
	N	15	15	15	15	15	15

*Marked *p*-values are significant (<0.05).

might be explained by the relationship between slope steepness and surface soil bulk density of the plot. A significant negative correlation was found between soil bulk density and slope gradient (Pearson $r = -0{\cdot}71$, $p = 0{\cdot}003$). It is probably due to the fact that those very steep 26·8% slope roads have less traffic than the less steep ones and, therefore, have less traffic-induced compaction. The effect of higher slope gradient on runoff response is likely to be reduced by lower soil bulk density.

Road surface soil loss was mainly determined by rainfall intensity and runoff rate, reflecting the effect of raindrop impact and flowing water acting together (Kinnell, 2005). The decline speeds of curves in Figure 3 illustrate the soil loss variability, which is controlled by the availability of road surface sediment (Ziegler *et al*., 2000a). Meanwhile, the unexpected effects of slope gradient and soil bulk density on runoff generation would in turn influence soil loss from road surface. The weak correlation between soil loss rate and slope might show that on some less-compacted steep road surfaces, runoff transport capacity was lower than that on highly compacted gentle slopes. Nevertheless, the low correlation does not imply that slope gradient contribute little to road surface soil loss. In fact, the extremely high soil loss rate on 26·8% slope established that with the increase of rainfall intensity and slope gradient, the raindrop-induced shear forces and the runoff flow velocity would increase, which in turn would intensify erosion (Assouline & Ben-Hur, 2006). Meanwhile, the rising function exponent of regression lines in Figure 4 also reflected the slope effect on road surface soil loss. The linear relationship in Figure 4 was similar with previous study that was reported by Huang (1995), and the power trend was comparable to that reported by Meyer & Harmon (1989). Analogous results have been reported by Cao *et al*. (2011) based on field rill overland flow simulation experiments. On their 26·8% slope plots, intensive soil losses were caused by head cutting, thereby leading to a power relationship with a relatively high exponent between soil detachment rate and slope gradient. These results established that slope gradient plays an important role in soil loss on unpaved road surface (Macdonald *et al*., 2001).

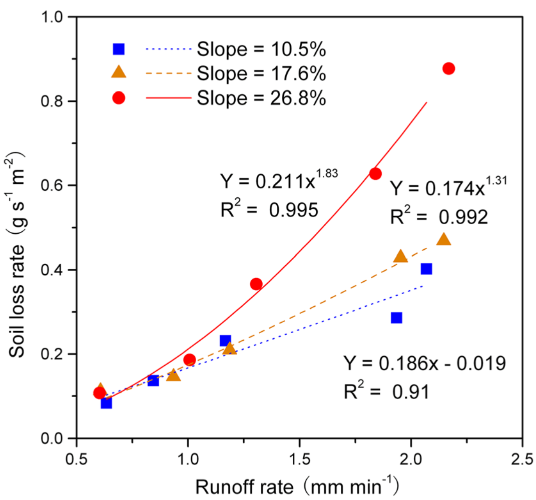

Figure 4. Road surface soil loss rates as functions of runoff rates. This figure is available in colour online at wileyonlinelibrary.com/journal/ldr.

Similar with that reported by Huang (1995), stream power that accounts for the effect of both slope steepness and runoff rate can be used for road surface soil loss prediction. The high determination coefficient of Equation 3 implied that the linear function could provide a reasonable estimation of road surface soil loss. The negative intercept suggested the existence of a threshold stream power for the initiation of the sediment transport process, a common concept in models based on the stream power theory. That is, soil erosion is considered to be a threshold phenomenon, and no soil was entrained when runoff energy was below the threshold stream power (Hairsine & Rose, 1992).

Road surface interrill erodibility calculated in this study was within the range ($1{\cdot}0$–$1{\cdot}8 \times 10^6\,\mathrm{kg\,s\,m^{-4}}$) that was reported by Foltz *et al*. (2009) on reopened forest road surfaces in northern Idaho, and it was very close to their dry run results ($1{\cdot}35 \times 10^6\,\mathrm{kg\,s\,m^{-4}}$). On the other hand, our result was lower than interrill erodibility of cultivated loess soil ($3{\cdot}14 \times 10^6\,\mathrm{kg\,s\,m^{-4}}$) that was reported by Yang *et al*. (2003). The result is consistent with that reported by Cao *et al*. (2011) for rill erosion conditions, implying that at given flow rate and slope gradient conditions, the compacted road surfaces are harder to erode than other land-use categories. However, it cannot be concluded that soil erosion risk on road surfaces is low. The sealed road surfaces could be a considerable source of runoff and have the potential to cause severe soil loss to nearby downstream regions. Furthermore, as reported both by this study and by Cao *et al*. (2011), road surfaces showed unique hydrological

Table V. Efficiency of models selected

	Equation	ME
Model 1	$D_i = 1335793 \times IQS_f$	0·814
Model 2	$D_i = 2215943 \times IQS$	0·914
Model 3	$D_i = 1321947 \times IQS^{2/3}$	0·893
Model 4	$D_i = 7475{\cdot}28 \times IQ^{1/2}S^{2/3}$	0·927

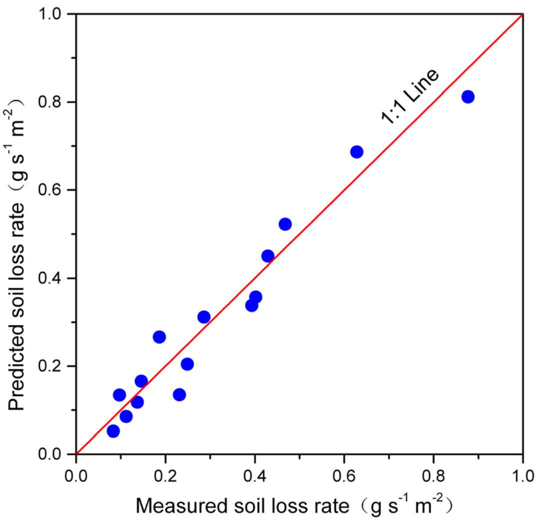

Figure 5. Comparison of measured and predicted soil loss rates. This figure is available in colour online at wileyonlinelibrary.com/journal/ldr.

characteristics and relatively intensive erosion on steep slope gradient. Hence, the soil loss from the steep road surfaces in watersheds of the Loess Plateau should be treated as a potentially very large contributor to total sediment lost source and should be evaluated precisely. Especially in the wet season, high-intensity storm would further aggravate road-related soil erosion risk. Future research should be conducted in a suitable temporal context of rainfall erosivity to obtain an accurate evaluation of road surface soil loss (Taguas *et al*., 2011).

CONCLUSIONS

Field rainfall simulation experiments on loess road surfaces were conducted under three slope gradients and five rainfall intensities. The results showed that loess road surfaces quickly generated runoff and produced a high runoff coefficient. During a rainstorm, road surface soil loss rate showed the first flush followed by a reduction with time as the loose materials were washed away. Rainfall intensity, initial soil moisture, and plots slope gradient played important roles in road surface runoff and erosion. Road surfaces showed unique hydrological characteristics and relatively intensive erosion on steep slopes.

Stream power can provide a precise estimation to loess road surface soil loss ($q_s = 0{\cdot}00008\omega - 0{\cdot}00079$, $R^2 = 0{\cdot}907$). Interrill erodibility following the WEPP model was calculated as being $1{\cdot}34 \times 10^6$ (kg s m^{-4}). On the basis of the comparison of four generally used interrill soil loss models, a new equation composed of rainfall intensity, surface flow discharge, and slope gradient was developed as $D_i = 12536{\cdot}15IQ^{1/2}S$. The results are helpful to develop erosion models and improve the accuracy of existing models based on physical properties for interrill soil loss prediction on loess road surfaces. Also, our results reveal that in order to minimize road-related sediment, a possible action is the designing of proper road drainage and reducing road slope.

ACKNOWLEDGEMENTS

Work reported in this paper is part of the projects 41101253 and 41071184 that were supported by the National Natural Science Foundation of China and project 2011BAD31B04-2 supported by the Key Technologies Research and Development Program of China. The authors gratefully thank Dr. Shuang Li and Ms. Rebecca May who kindly helped us to improve the language of this paper. We are also grateful for the valuable comments and suggestions from two anonymous reviewers.

REFERENCES

Al-Awadhi JM. 2011. A case assessment of the mechanisms involved in human-induced land degradation in northeastern Kuwait. *Land Degradation & Development* **22**: 2–11. DOI: 10.1002/ldr.1090.

Arnáez J, Larrea V, Ortigosa L. 2004. Surface runoff and soil erosion on unpaved forest roads from rainfall simulation tests in northeastern Spain. *Catena* **57**: 1–14.

Assouline S, Ben-Hur M. 2006. Effects of rainfall intensity and slope gradient on the dynamics of interrill erosion during soil surface sealing. *Catena* **66**: 211–220.

Bulygin SY, Nearing MA, Achasov AB. 2002. Parameters of interrill erodibility in the WEPP model. *Eurasion Soil Science* **35**: 1237–1242.

Cao LX, Zhang KL, Dai HL, Guo ZL. 2011. Modeling soil detachment on unpaved road surfaces on the Loess Plateau. *Transactions of the ASABE* **54**: 1377–1384.

Cao LX, Zhang KL, Zhang W. 2009. Detachment of road surface soil by flowing water. *Catena* **76**: 155–162.

Cerdà A. 1998. Relationship between climate and soil hydrological and erosional characteristics along climatic gradients in Mediterranean limestone areas. *Geomorphology* **25**: 123–134.

Cerdà A. 2007. Soil water erosion on road embankments in eastern Spain. *Science of the Total Environment* **378**: 151–155.

Cerdà A, Giménez-Morera A, Bodí MB. 2009. Soil and water losses from new citrus orchards growing on sloped soils in the western Mediterranean basin. *Earth Surface Processes and Landforms* **34**: 1822–1830.

Commandeur PR. 1992. Soil erosion studies using rainfall simulation on forest harvested areas in British Columbia. *Erosion, Debris Flows and Environment in Mountain Regions: Proceedings of the International Symposium on Chengdu, China*, 21–28.

Croke J, Mockler S. 2001. Gully initiation and road-to-stream linkage in a forested catchment, southeastern Australia. *Earth Surface Processes and Landforms* **26**: 205–217.

Croke J, Hairsine P, Fogarty P. 1999. Sediment transport, redistribution and storage on logged forest hillslopes in south-eastern Australia. *Hydrological Processes* **13**: 2705–2720.

Darboux F, Davy P, Gascuel-Odoux C, Huang C. 2001. Evolution of soil surface roughness and flowpath connectivity in overland flow experiments. *Catena* **46**: 125–139.

Desprats JF, Raclot D, Rousseau M, Cerdan O, Garcin M, Le Bissonnais Y, Ben Slimane A, Fouche J, Monfort-Climent D. 2013. Mapping linear erosion features using high and very high resolution satellite imagery. *Land Degradation & Development* **24**: 22–32. DOI: 10.1002/ldr.1094.

Dunne T. 1979. Sediment yield and landuse in tropical catchments. *Journal of Hydrology* **42**: 281–300.

Elliot WJ, Foltz RB, Luce CH. 1995. Validation of the Water Erosion Prediction Project (WEPP) model for low-volume forest roads. *Proceedings of the 6th International Conference on Low-volume Roads*, Washington, DC; 178–186.

Flanagan DC, Nearing MA. 1995. USDA-Water Erosion Prediction Project: hillslope profile and watershed model documentation, NSERL Rep. No. 10, National Soil Erosion Research Laboratory, USDA ARS, West Lafayette, IN.

Foltz RB, Copeland NS, Elliot WJ. 2009. Reopening abandoned forest roads in northern Idaho, USA: quantification of runoff, sediment concentration, infiltration, and interrill erosion parameters. *Journal of Environmental Management* **90**: 2542–2550.

Foster IDL, Rowntree KM, Boardman J, Mighall TM. 2012. Changing sediment yield and sediment dynamics in the Karoo Uplands, South Africa:

post-European impacts. *Land Degradation & Development* **23**: 508–522. DOI: 10.1002/ldr.2180.

Fu BJ, Wang J, Chen LD, Qiu Y. 2003. The effect of land use on soil moisture variation in the Danangou catchment of the Loess Plateau of China. *Catena* **54**: 197–213.

Hairsine PB, Rose CW. 1992. Modeling water erosion due to overland flow using physical principles, 1. Sheet flow. *Water Resources Research* **28**: 237–243.

Huang CH. 1995. Empirical analysis of slope and runoff for sediment delivery from interrill areas. *Soil Science Society of America Journal* **59**: 982–990.

IBM Corp. Released 2010. *IBM SPSS statistics for Windows, version 19.0*. Armonk, NY: IBM Corp.

Jordán A, Martínez-Zavala L. 2008. Soil loss and runoff rates on unpaved forest roads in southen Spain after simulated rainfall. *Forest Ecology and Management* **255**: 913–919.

Jordán A, Martínez-Zavala L, Bellinfante N. 2009. Impact of different parts of unpaved forest roads on runoff and sediment yield in a Mediterranean area. *Science of the Total Environment* **407**: 937–944.

Kinnell PIA. 1993. Runoff as a factor influencing experimentally determined interrill erodibilities. *Australian Journal of Soil Research* **31**: 333–342.

Kinnell PIA. 2005. Raindrop-impact-induced erosion processes and prediction: a review. *Hydrological Processes* **19**: 2815–2844.

Leh M, Bajwa S, Chaubey I. 2013. Impact of land use change on erosion risk: an integrated remote sensing, geographic information system and modeling methodology. *Land Degradation & Development*. DOI: 10.1002/ldr.1137.

Liu BY, Nearing MA, Risse LM. 1994. Slope gradient effects on soil loss for steep slopes. *Transactions of the ASAE* **37**: 1835–1840.

Liu G, Tian FX, Warrington DN, Zheng SQ, Zhang Q. 2010. Efficacy of grass for mitigating runoff and erosion from an artificial loessial earthen road. *Transactions of the ASABE* **53**: 119–125.

Luce CH, Black TA. 1999. Sediment production from forest roads in western Oregon. *Water Resources Research* **35**: 2561–2570.

MacDonald LH, Sampson RW, Anderson DM. 2001. Runoff and road erosion at the plot and road segment scale, St. John, U S Virgin Islands. *Earth Surface Processes and Landforms* **26**: 1–22.

Martínez-Zavala L, López AJ, Bellinfante N. 2008. Seasonal variability of runoff and soil loss on forest road backslopes under simulated rainfall. *Catena* **74**: 73–79.

Meyer LD. 1994. Rainfall simulators for soil erosion research. In *Soil erosion research methods*, 2nd edn, Lal R (ed.). Soil and Water Conservation Society (Ankeny) and St Lucie Press: Delray Beach, FL; 83–104.

Meyer LD, Harmon WC. 1979. Multiple intensity rainfall simulator for erosion research on row side slopes. *Transactions of the ASAE* **22**: 100–103.

Meyer LD, Harmon WC. 1989. How row-sideslope length and steepness affect side-slope erosion. *Transactions of the ASAE* **32**: 639–644.

Morgan RPC. 2005. *Soil erosion and conservation*, 3rd edn. Blackwell Publishing: Oxford.

Nash JE, Sutcliffe JE. 1970. River flow forecasting through conceptual models, part 1-a discussion of principles. *Journal of Hydrology* **10**: 282–290.

Nearing MA, Norton LD, Bulgakov DA, Larionov GA, West LT, Dontsova KM. 1997. Hydraulics and erosion in eroding rills. *Water Resources Research* **33**: 865–876.

Posthumus H, Deeks LK, Fenn I, Rickson RJ. 2011. Soil conservation in two English catchments: linking soil management with policies. *Land Degradation & Development* **22**: 97–110. DOI: 10.1002/ldr.987.

Reid LM, Dunne T. 1984. Sediment production from forest road surfaces. *Water Resources Research* **20**: 1753–1761.

Sheridan GJ, Noske PJ, Lane PN, Sherwin CB. 2008. Using rainfall simulation and site measurements to predict annual interrill erodibility and phosphorus generation rates from unsealed forest roads: validation against in-situ erosion measurements. *Catena* **73**: 49–62.

Song GQ, Li LT, Guo FG, Zhao ML. 1989. Land classification of experiment and exemplary areas on the Loess Plateau. *Memoir of Northwestern Institute of Soil and Water Conservation, Academia Sinica and Ministry of Water resources* (in Chinese with English abstract) **10**:1–13.

Taguas EV, Carpintero E, Ayuso JL. 2011. Assessing land degradation risk through the long-term analysis of erosivity: a case study in southern Spain. *Land Degradation & Development* **24**: 179–187. DOI: 10.1002/ldr.1119.

Tømmervik H, Johansen B, Høgda KA, Strann KB. 2012. High-resolution satellite imagery for detection of tracks and vegetation damage caused by all-terrain vehicles (ATVs) in Northern Norway. *Land Degradation & Development* **23**: 43–52. DOI: 10.1002/ldr.1047.

Xie Y, Lin XJ, Liu YN, Zheng YZ, Liu BY, Zhang GH. 2008. Calibration of simulated rainfall intensity and its spatial distribution for trough rainfall simulator. *Bulletin of Soil and Water Conservation* (in Chinese with English abstract) **28**: 1–6.

Xu XX, Ju TJ, Zheng SQ. 2007. Field study on biological road erosion in loess hilly region. *Journal of Agro-Environment Science* (in Chinese with English abstract) **26**: 934–938.

Xu XL, Liu W, Kong YP, Zhang KL, Yu B, Chen JD. 2009. Runoff and water erosion on road side-slopes: effects of rainfall characteristics and slope length. *Transportation Research Part D* **14**: 497–501.

Yang MY, Liu PL, Tian JL. 2003. Soil erosion processes on cultivated slope on Loess Plateau using 7Be tracer. *Journal of Soil Water Conservation* (in Chinese with English abstract) **17**: 28–30.

Zhang XC, Nearing MA, Miller WP, Norton LD, West LT. 1998. Modeling interrill sediment delivery. *Soil Science Society of America Journal* **62**: 438–444.

Zhao GJ, Mu XM, Wen ZM, Wang F, Gao P. 2013. Soil erosion, conservation and eco-environment changes in the Loess Plateau of China. *Land Degradation & Development*. DOI: 10.1002/ldr.2246.

Ziegler AD, Giambelluca TW, Sutherland RA. 2001. Erosion prediction on unpaved mountain roads in northern Thailand: validation of dynamic erodibility modeling using KINEROS2. *Hydrological Processes* **15**: 337–358.

Ziegler AD, Sutherland RA, Giambelluca TW. 2000a. Partitioning total erosion on unpaved roads into splash and hydraulic components: the roles of interstorm surface preparation and dynamic erodibility. *Water Resources Research* **36**: 2787–2791.

Ziegler AD, Sutherland RA, Giambelluca TW. 2000b. Runoff generation and sediment production on unpaved roads, footpaths and agricultural land surfaces in northern Thailand. *Earth Surface Processes and Landforms* **25**: 519–534.